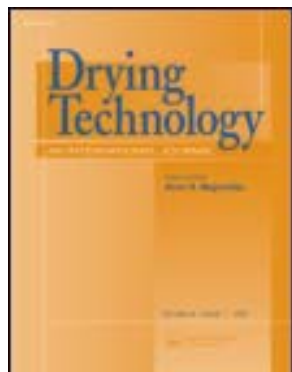


This article was downloaded by: [Thammasat University]

On: 03 July 2011, At: 21:26

Publisher: Taylor & Francis

Informa Ltd Registered in England and Wales Registered Number: 1072954 Registered office: Mortimer House, 37-41 Mortimer Street, London W1T 3JH, UK



Drying Technology

Publication details, including instructions for authors and subscription information:

<http://www.tandfonline.com/loi/ldrt20>

Analysis of Heat-Mass Transport and Pressure Buildup Induced inside Unsaturated Porous Media Subjected to Microwave Energy Using a Single (TE₁₀) Mode Cavity

Nattawut Suwannapum^a & Phadungsak Rattanadecho^a

^a Research Center of Microwave Utilization in Engineering (RCME), Department of Mechanical Engineering, Faculty of Engineering, Thammasat University, Pathumthani, Thailand

Available online: 27 Jun 2011

To cite this article: Nattawut Suwannapum & Phadungsak Rattanadecho (2011): Analysis of Heat-Mass Transport and Pressure Buildup Induced inside Unsaturated Porous Media Subjected to Microwave Energy Using a Single (TE₁₀) Mode Cavity, *Drying Technology*, 29:9, 1010-1024

To link to this article: <http://dx.doi.org/10.1080/07373937.2010.548110>

PLEASE SCROLL DOWN FOR ARTICLE

Full terms and conditions of use: <http://www.tandfonline.com/page/terms-and-conditions>

This article may be used for research, teaching and private study purposes. Any substantial or systematic reproduction, re-distribution, re-selling, loan, sub-licensing, systematic supply or distribution in any form to anyone is expressly forbidden.

The publisher does not give any warranty express or implied or make any representation that the contents will be complete or accurate or up to date. The accuracy of any instructions, formulae and drug doses should be independently verified with primary sources. The publisher shall not be liable for any loss, actions, claims, proceedings, demand or costs or damages whatsoever or howsoever caused arising directly or indirectly in connection with or arising out of the use of this material.

Analysis of Heat–Mass Transport and Pressure Buildup Induced inside Unsaturated Porous Media Subjected to Microwave Energy Using a Single (TE₁₀) Mode Cavity

Nattawut Suwannapum and Phadungsak Rattanadecho

Research Center of Microwave Utilization in Engineering (RCME), Department of Mechanical Engineering, Faculty of Engineering, Thammasat University, Pathumthani, Thailand

This article presents the two-dimensional numerical analysis of heat and mass transport and pressure built up inside an unsaturated porous packed bed under microwave energy at a frequency of 2.45 GHz using a rectangular waveguide (TE₁₀ mode). The unsaturated porous packed beds were composed by glass beads, water, and air. The samples were prepared by compacting uniformly with various thicknesses $\delta = 30, 50,$ and 80 mm and particle sizes $d = 0.15$ mm (fine packed bed) and 0.4 mm (coarse packed bed), respectively. A proposed model used to investigate heat–mass transport and pressure buildup phenomena inside the porous packed bed in which the rectangular waveguide with varying glass bead sizes and sample thicknesses was inserted. The results show that the effect of particle sizes and thicknesses of porous packed bed are primary factors determining heat and mass transport with multiphase flow. These findings can explain the phenomena taking place inside unsaturated porous media in a microwave drying process using a rectangular waveguide.

Keywords Microwave drying; Numerical; Particle size; Porous packed bed; Rectangular sample thickness; Waveguide

INTRODUCTION

In the past decade, many successful examples of microwave heating and drying applications have been appeared in the recent literature.^[1–7]

In theoretical analysis, microwave power absorbed is generally assumed to decay exponentially into the absorbed material as Lambert's law. However, this law is valid for samples of large dimensions for which the depth of sample is much larger than the penetration depth, but it is not valid for small samples for which the depth of the sample is smaller than the penetration depth.^[1] Therefore, analysis of the electromagnetic field within a small sample cloud was obtained by solving Maxwell's equations. Two-dimensional models by solving Maxwell's equations have been used for study numerous heating processes in microwave applicator configurations.^[8,9]

Correspondence: Phadungsak Rattanadecho, Research Center of Microwave Utilization in Engineering (RCME), Department of Mechanical Engineering, Faculty of Engineering, Thammasat University, 99 Moo 18, Pathumthani 12120, Thailand; E-mail: ratphadu@engr.tu.ac.th

However, most previous investigations considered simulations of microwave heating in homogeneous material.

Theoretical analysis of heat and mass transfer in porous materials has been studied for several decades. Most theories based on Whitaker's theory have been proposed to explain the physical phenomena of drying process in porous materials. Those theories have three main difference fundamental to describing porous materials.

1. One variable: This fundamental uses one single diffusion equation and is used for simple configurations.
2. Two variables: This fundamental uses two independent variables (temperature and moisture content). In this model, the effect of pressure buildup can be neglected. This fundamental can describe the most important feature of drying at low temperature.
3. Three variables: This fundamental uses three independent variables (temperature, moisture content, and pressure buildup). This model provides better phenomena detail than a two variable model because it can describe all drying behaviors. Furthermore, it can also be used in case of high-temperature convective drying, vacuum drying, radio-frequency (RF)/vacuum drying, etc.

However, most of the literature has targeted one or two variables in case of conventional drying process^[10–12] because they are easier to discretize and solve than three variables. For example, a few studies that used three variable parameters are Perre and Turner^[8] and Rattanadecho et al.^[13]

Nevertheless, a few of researchers have studied the interaction between microwave energy and heat–mass transfer of porous material, such as microwave heating and drying process.^[8,14–20] Additionally, most previous works have not mentioned two-dimensional pressure buildup and flow field inside porous materials with varying particle sizes.

A recent work carried out a systematic investigation on heat–mass transport and pressure buildup phenomena during the drying process in a uniform porous packed bed by microwave energy that extends from Rattanadecho et al.'s^[21] work (the effect of pressure buildup in mathematical modeling was

neglected) in which the effect of particle sizes and thicknesses of porous packed bed are primary factors determining heat and mass transport with multiphase flow. Due to the limited amount of theoretical and experimental analysis on microwave drying of uniform porous materials, the various effects are not fully understood and a number of critical issues remain unresolved. In this study, mathematical models are numerically solved and compared with experiments. The effects of sample thickness and sample size on overall heat and multiphase flow are also investigated in detail.

The results presented here provide a basis for understanding the fundamentals of microwave drying of multi-layered porous media.

MATHEMATICAL FORMULATION

Dielectric Properties

The problem of microwave drying directly relates to electromagnetic fields and temperature and moisture distributions within the absorbed material. Therefore, understanding the absorbed material's dielectric properties is an essential primary factor for theoretical prediction.

In this study, the effects on overall drying kinetic were investigated by selecting the dielectric properties (ϵ_r) as a function of water saturation (s) and temperature. For the combination of water saturation and temperature of dielectric properties, the volume fractions of water saturation, water vapor, and solid particles in porous material were taken into account as follows:

$$\epsilon'_r(s, T) = \phi s \epsilon'_{rl} + \phi(1-s) \epsilon'_{rg} + (1-\phi) \epsilon'_{rp} \quad (1)$$

$$\epsilon''_r(s, T) = \phi s \epsilon''_{rl} + \phi(1-s) \epsilon''_{rg} + (1-\phi) \epsilon''_{rp} \quad (2)$$

where ϵ'_r is the real part of relative permittivity, ϵ''_r is the imaginary part of relative permittivity, ϕ is the porosity of porous material, and subscripts l , g , and p represent liquid, gas, and solid particle, respectively.

Furthermore, the relative permittivity and loss tangent coefficient of water at a frequency of 2.45 GHz can be written in empirical formula as a temperature function:^[21]

$$\epsilon'_{rl}(T) = (88.15 - 0.414T + (0.131 \times 10^{-2})T^2 - (0.046 \times 10^{-4})T^3) \quad (3)$$

$$\tan \delta_l(T) = (0.323 - (9.499 \times 10^{-3})T + (1.27 \times 10^{-4})T^2 - (6.13 \times 10^{-7})T^3) \quad (4)$$

where $\tan \delta$ is the loss tangent coefficient, which can be expressed as follows:^[22]

$$\tan \delta = \frac{\epsilon''_r(s, T)}{\epsilon'_r(s, T)} \quad (5)$$

Maxwell's Equation

The basic equations for analyzing the electromagnetic fields are the well-known Maxwell's relations. For the microwave of TE₁₀ mode, the governing equations can be written in terms of the component notations of electric and magnetic field intensities:^[21]

$$\frac{\partial E_y}{\partial z} = \mu \frac{\partial H_x}{\partial t} \quad (6)$$

$$\frac{\partial E_y}{\partial x} = -\mu \frac{\partial H_z}{\partial t} \quad (7)$$

$$-\left(\frac{\partial H_z}{\partial x} - \frac{\partial H_x}{\partial z}\right) = \sigma E_y + \epsilon \frac{\partial E_y}{\partial t} \quad (8)$$

where permittivity ϵ , magnetic permeability μ , and electric conductivity σ are given by:

$$\epsilon = \epsilon_0 \epsilon_r, \quad \mu = \mu_0 \mu_r, \quad \sigma = 2\pi f \epsilon \tan \delta \quad (9)$$

where f is the frequency of the microwave, $\tan \delta$ is the dielectric loss tangent, and ϵ_r and μ_r are the relative permittivity and relative magnetic permeability, respectively.

Analysis of Heat and Mass Transport

A schematic of the porous packed bed model is shown in Fig. 1. Based on the conservation of mass and energy in capillary porous materials, the governing equation of mass and energy of all phases can be derived using the volume-averaging technique.^[23] The surface of the sample is exposed to the external drying conditions. Microwaves in the form of a plane wave are also incident to this surface. In addition, other surfaces are insulated and the heat and mass fluxes are set equal to zero.

Moisture Transport Equation

Considering Darcy's law and Fick's law and assuming that the phenomenon of moisture transport in the sample is described by the mass balance equations of water and water vapor, the moisture transport equation in two-dimensional scalar forms can be expressed as follows:

$$\phi \frac{\partial}{\partial t} \{ \rho_l s + \rho_v (1-s) \} + \frac{\partial}{\partial x} \left[\rho_l \frac{KK_{rl}}{\mu_l} \left(\frac{\partial p_c}{\partial x} - \frac{\partial p_g}{\partial x} \right) + \rho_v \frac{KK_{rg}}{\mu_g} \left(-\frac{\partial p_g}{\partial x} \right) - D_m \frac{\partial \rho_v}{\partial x} \right] + \frac{\partial}{\partial z} \left[\rho_l \frac{KK_{rl}}{\mu_l} \left(\frac{\partial p_c}{\partial z} - \frac{\partial p_g}{\partial z} + \rho_l g_z \right) + \rho_v \frac{KK_{rg}}{\mu_g} \left(-\frac{\partial p_g}{\partial z} + \rho_g g_z \right) - D_m \frac{\partial \rho_v}{\partial z} \right] = 0 \quad (10)$$

Total Pressure Equation

Considering Darcy's law and Fick's law and assuming that the gaseous phase is an ideal mixture of perfect gases,

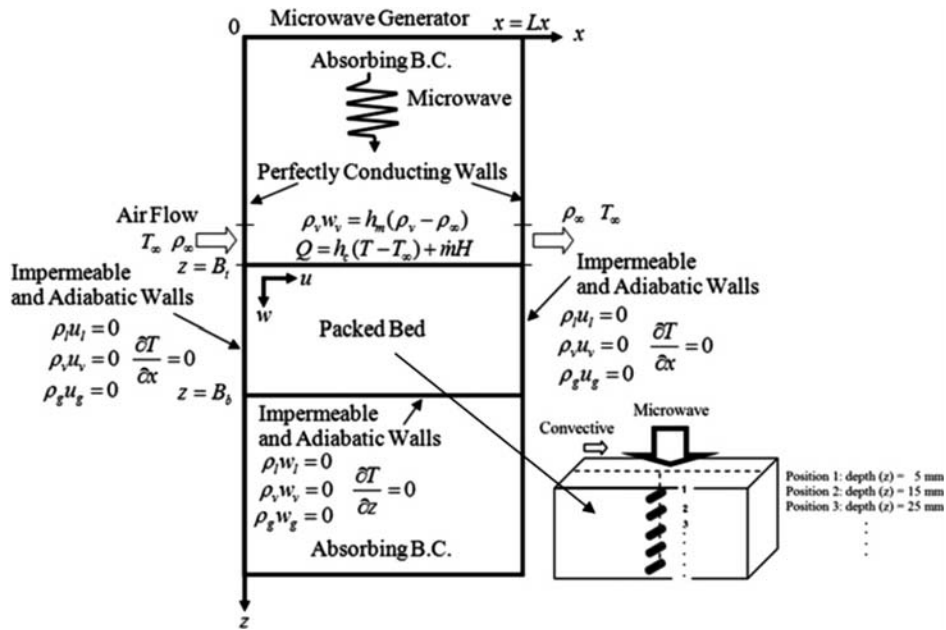


FIG. 1. Physical model and measured point.

the pressure equation in two-dimensional scalar forms can be expressed as follows:

$$\phi \frac{\partial}{\partial t} \{ \rho_a (1 - s) \} + \frac{\partial}{\partial x} \left[\rho_a \frac{KK_{rg}}{\mu_g} \left(-\frac{\partial p_g}{\partial x} \right) - D_m \frac{\partial \rho_a}{\partial x} \right] + \frac{\partial}{\partial z} \left[\rho_a \frac{KK_{rg}}{\mu_g} \left(-\frac{\partial p_g}{\partial z} + \rho_g g_z \right) - D_m \frac{\partial \rho_a}{\partial z} \right] = 0. \quad (11)$$

Equilibrium Relations and State Equations

The system of conservation equations obtained for multiphase transport mode requires a constitutive equation for relative permeabilities K_r , capillary pressure p_c , and capillary pressure functions (Leverett functions). This typical set of constitutive relationships for liquid and gas systems is given by:

$$K_{rl} = s_e^3 \quad (12)$$

$$K_{rg} = (1 - s_e)^3 \quad (13)$$

where s_e is the effective water saturation considered the irreducible water saturation s_{ir} and is defined by:

$$s_e = \frac{s - s_{ir}}{1 - s_{ir}}. \quad (14)$$

The capillary pressure p_c is further assumed to be adequately represented by Leverett's well-known $J(s_e)$ functions; the relationship between the capillary pressure

and the water saturation is defined by using Leverett functions $J(s_e)$:

$$p_c = p_g - p_l = \frac{\xi}{\sqrt{K/\phi}} J(s_e) \quad (15)$$

in which ξ is the gas-liquid interfacial tension, where $J(s_e)$ was correlated capillary pressure data obtained by Leverett as follows to give $J(s_e)$:

$$J(s_e) = 0.325(1/s_e - 1)^{0.217}. \quad (16)$$

Energy Balance Equation

Thermal equilibrium among the water, gas, and matrix at any specific place in the unsaturated packed bed were assumed. Considering the enthalpy transport, heat conduction, latent heat transport, and volumetric heat generation, the energy balance equation is then represented by:

$$\frac{\partial}{\partial t} [(\rho C_p)_T T] + \frac{\partial}{\partial x} [\{ \rho_l C_{pl} u_l + (\rho_a C_{pa} + \rho_v C_{pv}) u_g \} T] + \frac{\partial}{\partial z} [\{ \rho_l C_{pl} w_l + (\rho_a C_{pa} + \rho_v C_{pv}) w_g \} T] + H_v \dot{m} = \frac{\partial}{\partial x} \left[\lambda_{eff} \frac{\partial T}{\partial x} \right] + \frac{\partial}{\partial z} \left[\lambda_{eff} \frac{\partial T}{\partial z} \right] + Q \quad (17)$$

where $(\rho C_p)_T$ is the effective heat capacitance of the water-gas matrix mixture:

$$(\rho C_p)_T = \rho_l C_{pl} \phi s + \rho_g C_{pg} \phi (1 - s) + \rho_p C_{pp} (1 - \phi) \quad (18)$$

and

$$\dot{m} = \frac{\partial}{\partial t} \{ \rho_v \phi (1 - s) \} + \frac{\partial}{\partial x} \left[-D_m \frac{\partial \rho_v}{\partial x} \right] + \frac{\partial}{\partial z} \left[\rho_v \frac{K K_{rg}}{\mu_g} \rho_g g_z - D_m \frac{\partial \rho_v}{\partial z} \right]. \quad (19)$$

H_v is the latent heat of evaporation, and λ_{eff} is the effective thermal conductivity and can be written in an empirical form as:^[21]

$$\lambda_{eff} = \frac{0.8}{1 + 3.78e^{-5.95s}}. \quad (20)$$

The rate of volumetric heat generation due to the absorption of microwaves, Q , is represented in the following equation^[21]:

$$Q = \omega \epsilon_r' E^2 = 2\pi f \epsilon_0 \epsilon_r' (\tan \delta) E_v^2. \quad (21)$$

Boundary and Initial Conditions

Corresponding to Fig. 1, there are two necessary types of boundary conditions for solutions of the governing equations. These types were applied on the permeable surface, impermeable surface, and layer interface. A detailed analysis of each condition follows.

Permeable Surface

The boundary conditions on the permeable surface, the exchange of energy at the open boundary, can be described in the following form:

$$-\lambda_{eff} \frac{\partial T}{\partial z} = h_c (T - T_\infty) + \dot{m} H_v. \quad (22)$$

Mass transfer at the permeable surface is modeled by a constant mass transfer coefficient, which is related to the local water vapor flux density:

$$\dot{m} = \rho_v w_v = h_m (\rho_v - \rho_{v\infty}) \quad (23)$$

where ρ_v is the density of water vapor at the permeable surface and $\rho_{v\infty}$ is reference vapor density in the gas phase surrounding the permeable surface.

The total pressure on the permeable surface can be defined as:

$$p_g = p_0. \quad (24)$$

Impermeable Surface

The boundary condition at the closed impermeable boundary expresses symmetry and without heat or mass

exchange can be described by the following equation

$$\frac{\partial T}{\partial x} = \frac{\partial T}{\partial z} = 0 \quad (25)$$

$$\frac{\partial u}{\partial x} = \frac{\partial u}{\partial z} = 0. \quad (26)$$

Numerical Solution

The heat, mass transfer, and total pressure equations were coupled to Maxwell's equations to find all phenomena within the sample.

In order to predict the electromagnetic field, a finite difference time domain (FDTD) method was applied.

In order to predict heat, mass transfer, and total pressure equations, a finite difference based on control volumes as describe by Patankar^[24] was applied.

Details of the computational schemes and strategy are illustrated in Fig. 2. The input data for porous physical

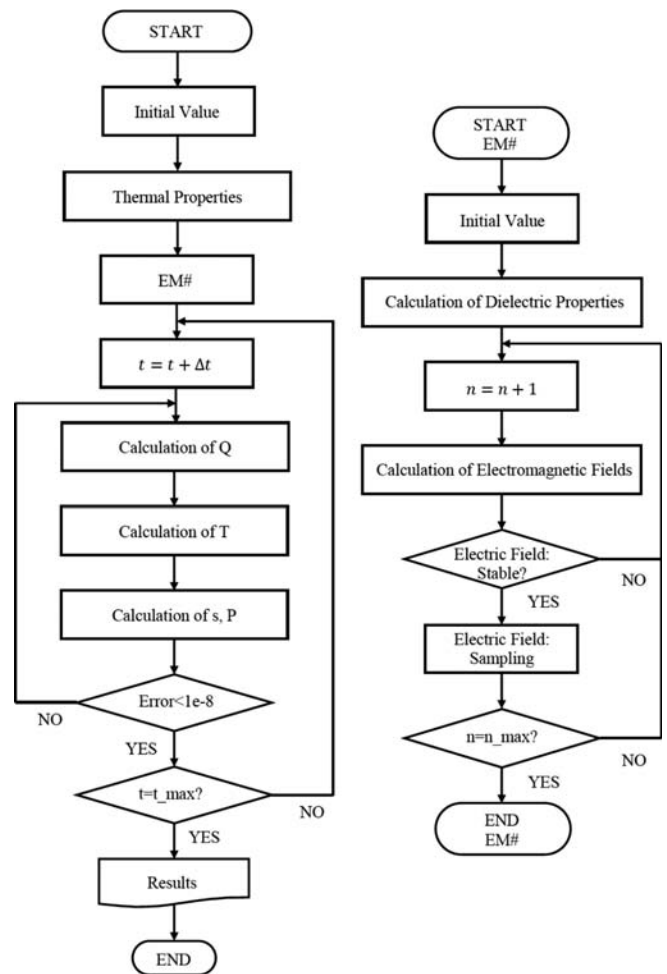


FIG. 2. Computational scheme.

TABLE 1
Porous physical properties of a packed bed used in the computations

Particle size d (mm.)	Porosity ϕ	Permeability K (m ²)
0.15 (F-bed)	0.385	8.41×10^{-12}
0.4 (C-bed)	0.371	3.52×10^{-11}

TABLE 2
Electromagnetic (dielectric) and thermophysical properties and drying conditions used in the computations

$\epsilon_0 = 8.85419 \times 10^{12}$ [F/m]	$\mu_0 = 4.0\pi \times 10^{-7}$ [H/m]
$\epsilon_{ra} = 1.0, \mu_{ra} = 1.0$	$\epsilon_{rp} = 5.1, \mu_{rp} = 1.0$
$\mu_{rl} = 1.0$	$\tan \delta_p = 0.01, \tan \delta_a = 0.00$
$\rho_a = 1.205$ [kg/m ³]	$\rho_l = 1,000$ [kg/m ³]
$\rho_p = 2,500$ [kg/m ³]	$C_{pa} = 1.007$ [kJ/(kg · K)]
$C_{pp} = 0.80$ [kJ/(kg · K)]	$C_{pp} = 4.186$ [kJ/(kg · K)]
$\lambda_l = 0.610$ [W/(m · K)]	$\lambda_p = 1.0$ [W/(m · K)]
$\lambda_a = 0.0256$ [W/(m · K)]	Initial saturation (s) = 0.6
$T_\infty = 25^\circ\text{C}$	$h_c = 20$ [W/(m ² · K)]
%RH = 55	$f = 2.45$ [GHz]
Power = 50 [watt]	$T_{\text{int}} = 25^\circ\text{C}$
$U_\infty = 1$ [m/s]	$p_{\text{int}} = p_{\text{atm}}$

properties of the fine-packed bed (F-bed) and coarse-packed bed (C-bed) are given in Table 1. Some of the input data for electromagnetic and thermophysical properties and drying conditions are given in Table 2.

RESULTS AND DISCUSSION

The simulated results for heat, multiphase flow, and pressure buildup in an unsaturated porous packed bed subjected to microwave energy were classified into two parts. Part one focused on the influence of different glass bead sizes (F-bed and C-bed). Part two focused on the influence of sample thicknesses. Additionally, details of the porous packed bed used for analyses are shown in Fig. 3.

The result of heat and mass transfer phenomena subjected to microwave energy inside unsaturated porous packed bed can be presented as follows.

Electric Field Simulation inside a Rectangular Waveguide

To understand the detailed structures of the electric field developed inside a rectangular waveguide, numerical simulations of the following four cases are presented:

1. The rectangular waveguide is empty. Dielectric properties are constant value inside all of rectangular waveguide which corresponds to air as shown in Fig. 4.

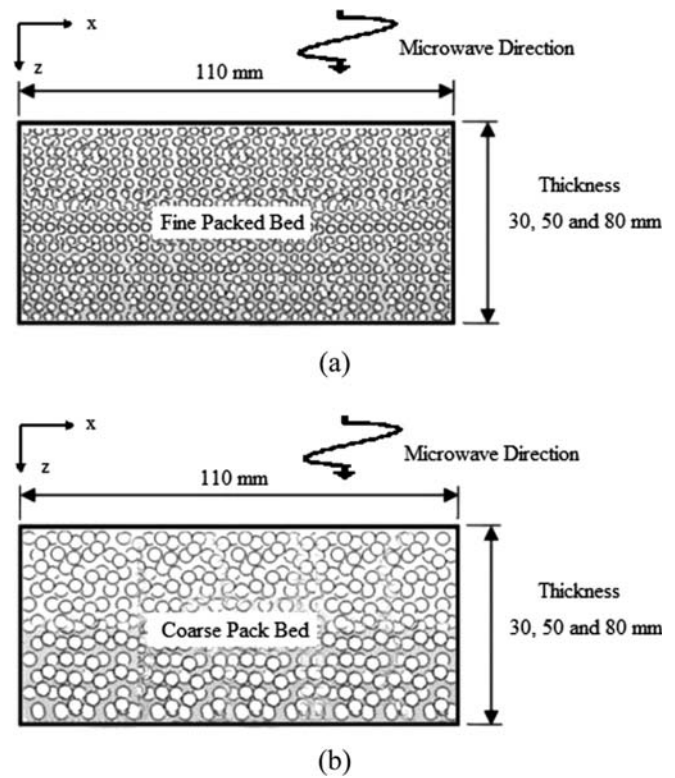


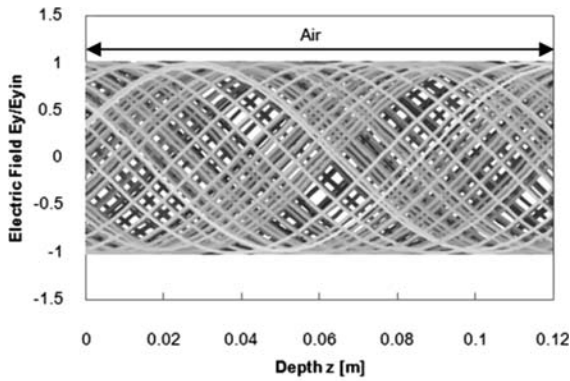
FIG. 3. Porous packed bed samples: (a) F-bed and (b) C-bed.

3. The rectangular waveguide is filled with a fine porous packed bed with various thicknesses during early heating (10 min) as shown in Figs. 5a and 6a.
4. The rectangular waveguide is filled with a fine porous packed bed with various thicknesses at heating time of 100 min as shown in Figs. 5b and 6b.
5. The rectangular waveguide is filled with a fine porous packed bed with various thicknesses at the end stage of heating as shown in Figs. 5c and 6c.

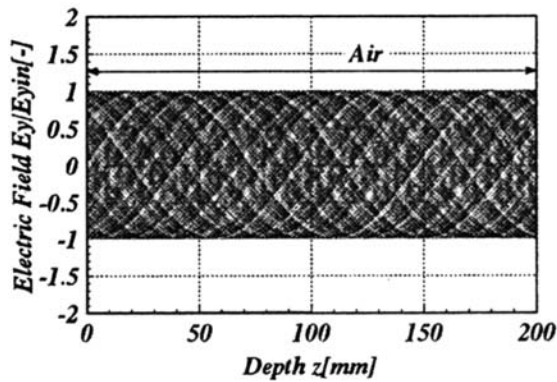
Figure 4 shows the stationary wave inside the empty rectangular waveguide with completely absorbed power at the end of the rectangular waveguide. It is observed that the electric field distribution displays a wavy behavior with an almost uniform amplitude along the rectangular waveguide. This result is similar to the results obtained by Rattanadecho et al.^[21]

Electric Field Distribution inside a Rectangular Waveguide at Various Elapsed Times

Figures 5a and 6a show the electric field distribution in the case of a fine porous packed bed having moist porous material (initial saturation = 0.6, F-bed) inserted in the rectangular waveguide at heating time of 10 min. Within the sample, the electric field attenuates due to energy absorption due to the sample's dielectric properties, and



(a)

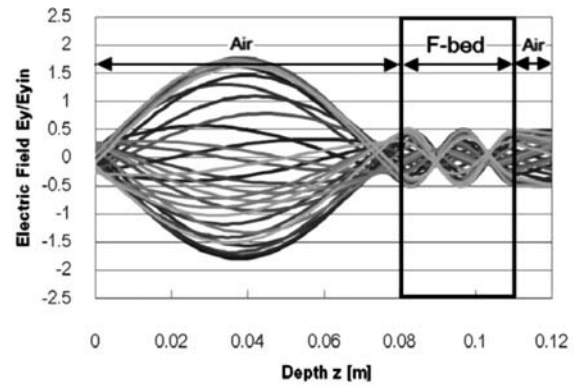


(b)

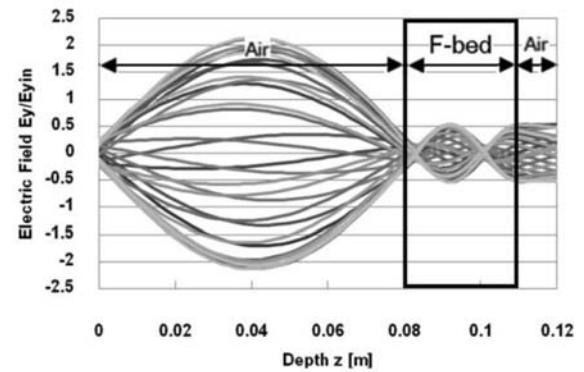
FIG. 4. Distribution of electric field in the case of an empty rectangular waveguide ($x = 55$ mm): (a) result of the present study and (b) result obtained by Rattandecho et al.^[21]

then the absorbed energy is converted to thermal energy, which increases the sample temperature. In the figure, the electric field within the sample is almost extinguished inside the sample which lead to short wavelength and amplitude of electric field because the sample at this period has a very high moisture content. However, focusing attention on the field pattern outside the sample, the strong standing wave with large amplitude is formed by interference between the forward wave and the reflection wave that occurred at the top surface of the sample.

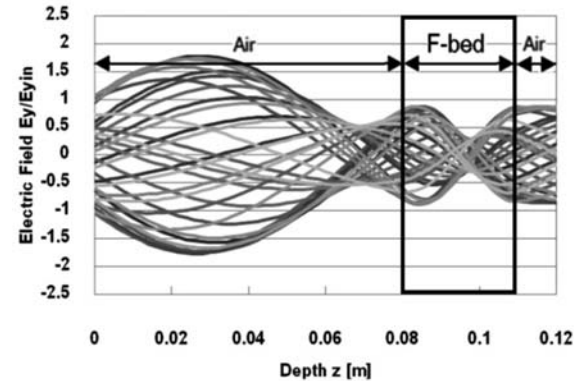
Figures 5b and 6b show the electric field distribution in the case of a fine porous packed bed having moist porous material (initial saturation = 0.6, F-bed) inserted in the rectangular waveguide and heating time of 100 min. Within the sample, the electric field attenuates due to energy absorption and changes to the thermal energy, which is similar to the early stage. However, the amplitude and wavelength at this time are higher and longer than in the early period. In the figure, the electric field is mostly extinguished inside the sample, but some remainder can penetrate from the sample to the air because the sample's dielectric properties are



(a)



(b)



(c)

FIG. 5. Distribution of electric field for the sample inserted in the rectangular wave guide (F-bed particle, 30 mm thicknesses): (a) early stage of drying time, (b) 100 min drying time, and (c) latter stage of drying time.

changed by a moisture content effect, and moisture at this time is lower than in the early stage due to the influence of thermal energy. Furthermore, some remainder of the electric field turned into the reflection wave at the bottom surface of the sample due to the difference of dielectric properties of the material (sample and air) that lead to a

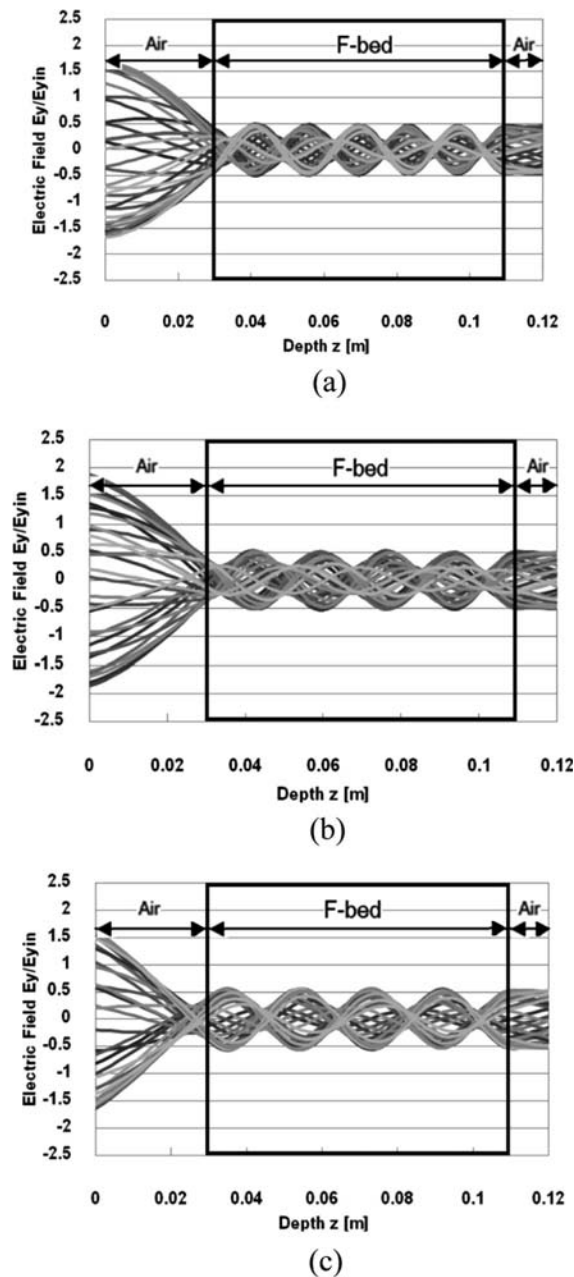


FIG. 6. Distribution of electric field for the sample inserted in the rectangular wave guide (F-bed particle, 80 mm thicknesses): (a) early stage of drying time, (b) drying time of 100 min, and (c) latter stage of drying time.

stronger standing wave within the sample than in the early stage. Moreover, the strong standing wave with large amplitude outside (top) the sample is formed by interference between the forward wave and the reflection wave, which is similar to the results in the early stage of heating.

Figure 5c and 6c show the wave distribution of the electric field when a dielectric material or sample (F-bed) is inserted in the rectangular waveguide at the end stage of

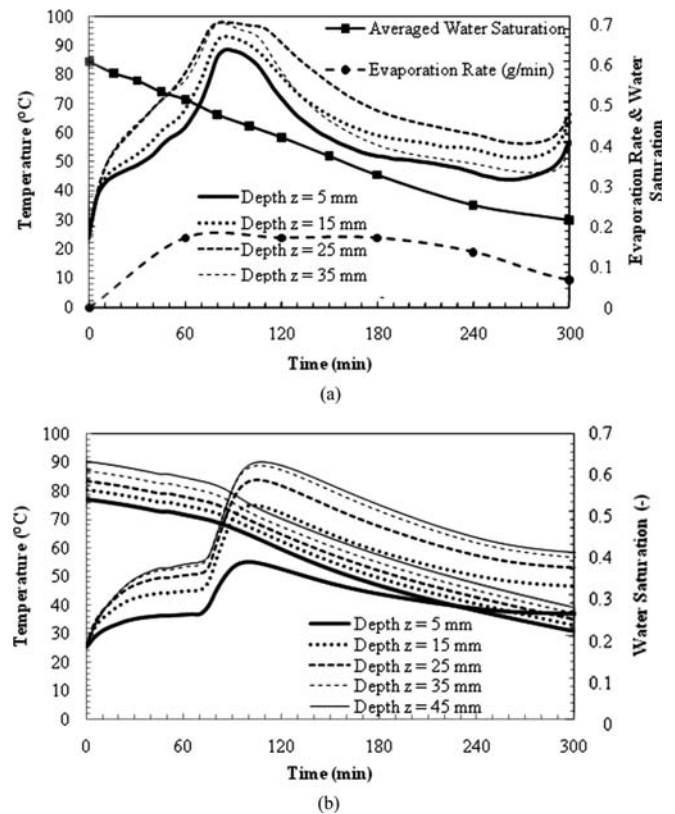


FIG. 7. Comparison of temperature and water saturation profiles and time with different depths (F-bed, sample thickness 50 mm): (a) experimental result and (b) simulated result.

heating. In this case, the effect of the reflection wave from the surface of the sample is reduced, which increases the large part of microwaves inside the sample. Consequently, the reflection and transmission components at each interface will contribute to the resonance of the standing waves configuration with the larger amplitude and the longer wavelength inside the sample compared with the previous cases.

Electric Field Distribution and Sample Thickness

Figures 5 and 6 show the electric field distribution at different sample thicknesses (30 and 80 mm, respectively). In the case of an 80-mm thickness layer packed bed, from the early stage until the end stage of heating time, the electric field distribution changes little because the thickness of the sample is close to the penetration depth, leading to a weaker standing wave than that of the case of a thin sample. As a result, lower thermal energy transformation induces low heat and mass transfer rates. Furthermore, dielectric properties (ϵ_r) as function of moisture content or water saturation (s) and temperature (T) represent the microwave power dissipation or electric field distribution. If the sample has a higher water saturation, it can be called high lossy material, which causes a weak standing wave in

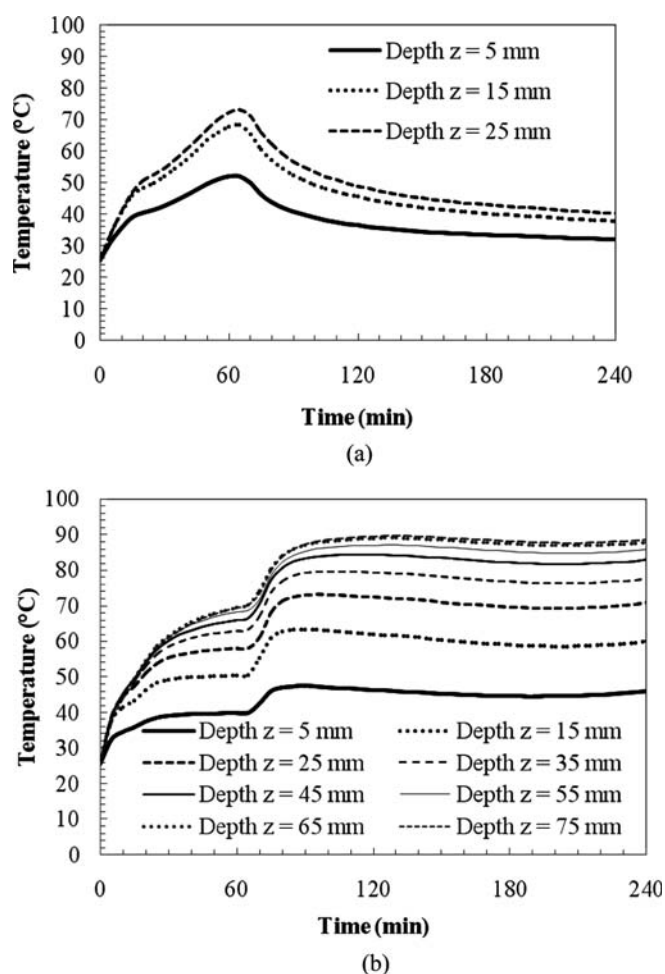


FIG. 8. Temperature profiles and time with different depths (F-bed): (a) sample thickness of 30 mm and (b) sample thickness of 80 mm.

the sample. This is because the wavelength in high lossy material is shorter than that in low lossy material and leads to low penetration depth in high lossy material. Therefore, a thick layer packed bed (80 mm), which has a low mass transfer rate, is still a high lossy material because the packed bed retains a high moisture content. On the other hand, the electric field distribution in the case of thin layer packed bed (30 mm) changes greatly because the thickness of the sample is possibly lower than the penetration depth, which causes a stronger standing wave than in the case of a thick sample. This leads to high microwave power absorbed (Q) and a strong standing wave, which has high electromagnetic field amplitude (E), that leads to a lot of thermal energy transformed as well as heat and mass transfer rates. Furthermore, a high driving force can reduce the moisture content and change dielectric properties of the sample from high lossy to low lossy material. Therefore, a thin layer packed bed can reduce moisture content or water saturation and increase temperature faster than the thick layer packed bed. However,

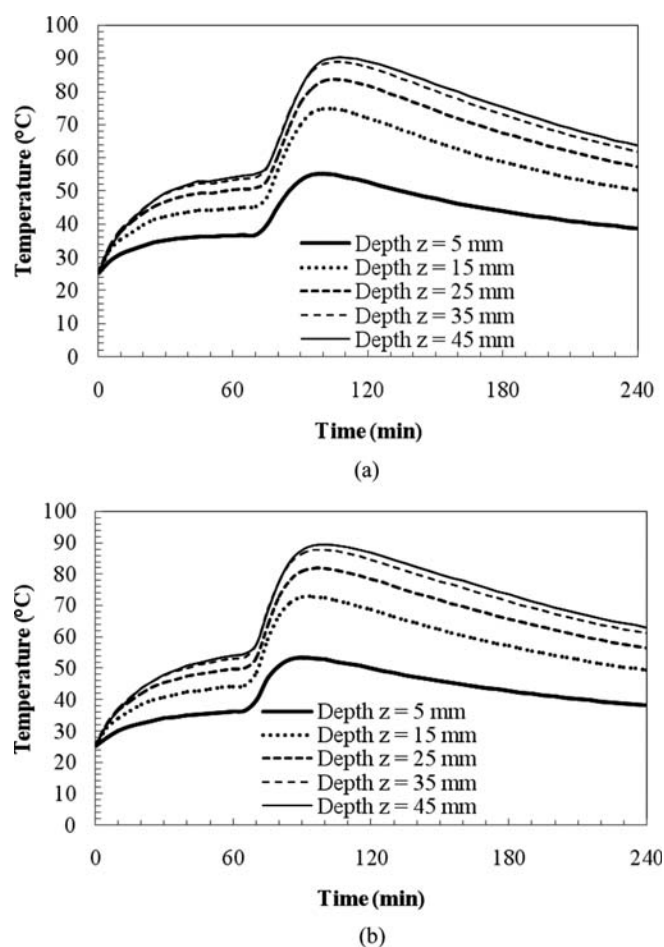


FIG. 9. Temperature profiles and time with different depths (sample thickness of 50 mm): (a) F-bed and (b) C-bed.

numerical simulations of the electromagnetic field in the F-bed and C-bed samples at the same thickness are not shown in this article because those have similar electric field pattern results.

Variation of the amplitude and wavelength of the electromagnetic field of thermal behavior in a typical porous packed bed is described by Eq. (21).

Temperature, Saturation, and Pressure Buildup Profiles Within the Samples

Numerical analysis results of a single-layered porous packed bed were compared with the temperature, saturation, and pressure distribution profiles between F-bed and C-bed conditions at the same boundary conditions.

In order to verify the numerical results, the predicted results of fine and coarse single layered porous packed bed at 30, 50, and 80 mm thicknesses were validated against the experimental data (no other work exists for validation). The predicted results are agreement with the experimental results for the cases of single-layer porous packed bed.

Some of the validated temperature and water saturation profile results are shown in Fig. 7. Nevertheless, with the limitations of the experimental apparatus, the pressure buildup and multiphase flow data inside the sample cannot be recorded; therefore, there are no pressure and multiphase flow experimental data for comparison with numerical data.

Figures 8 and 9 show the numerical result of the temperature profile versus elapsed time at various sample thicknesses (30, 50, and 80 mm). As shown in Figs. 8 and 9, microwave energy induces a higher temperature inside the sample than at the surface because microwave energy can be transmitted directly into the sample and transformed to thermal energy inside the sample. After starting microwave heating, the temperature inside the sample is rapidly increased by microwave energy, whereas the surface temperature remains cold due to the cooling effect of surrounding air. At the same time, the evaporation at the surface of the sample takes place at a lower temperature due to evaporative cooling. After 30 min of heating, the temperature inside the sample increased slowly compared with the beginning heating time due to the coupling effect of evaporative cooling near the surface and dielectric properties of the samples that are functions of moisture

content and temperature. However, the temperature inside the samples increased rapidly until the highest temperature point due to the effect of stronger standing wave with longer wavelength inside the low moisture sample that cause higher microwave power absorption than in the early stage of heating. After the highest temperature point in the heating process, the temperature is slowly decreased until the end of the process because moisture content has been removed gradually from the sample (the sample was changed from high lossy material to low lossy material). The effect of sample thickness is presented clearly in Figs. 8a, 8b, and 9a. These results show that the temperature profile of the thin layer packed beds differs from the thick layer packed beds because the sample thickness affects the electromagnetic wave pattern inside the cavity and sample as explained in the previous section. The thin sample can induce a resonance effect or strong standing wave more easily than that of the thick sample, which corresponds to a greater effect of microwave power absorbed and thermal energy transformation inside the sample.

From Figs. 9a and 9b, the effect of particle size on the temperature profile is not clearly seen in the packed bed.

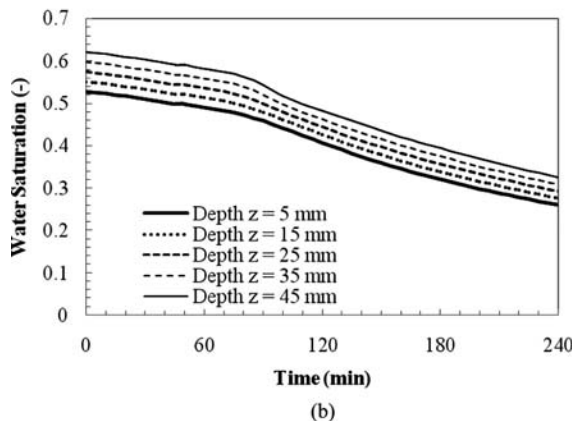
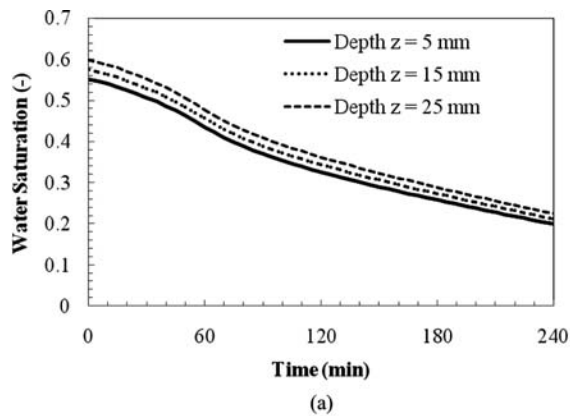


FIG. 10. Water saturation profiles and time with different depths (F-bed): (a) sample thickness of 30 mm and (b) sample thickness of 50 mm.

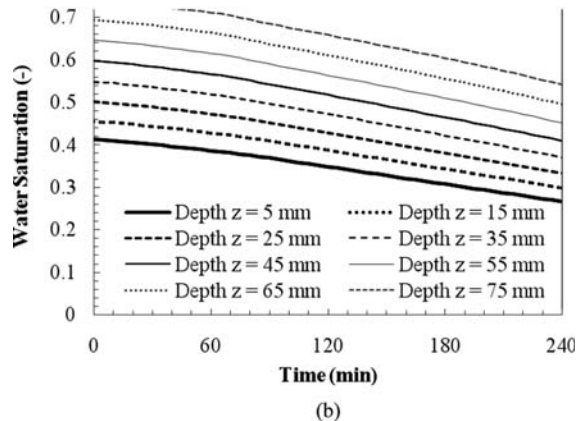
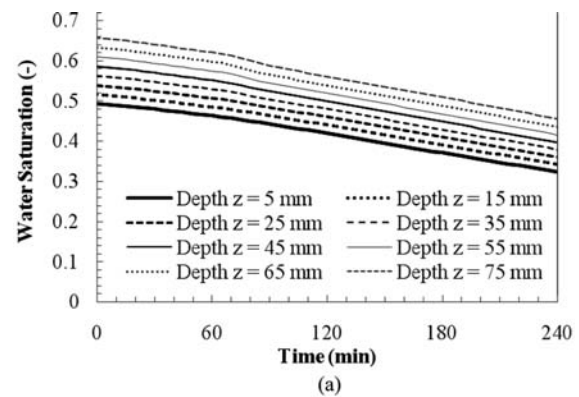


FIG. 11. Water saturation profiles and time with different depths (sample thickness of 80 mm): (a) F-bed and (b) C-bed.

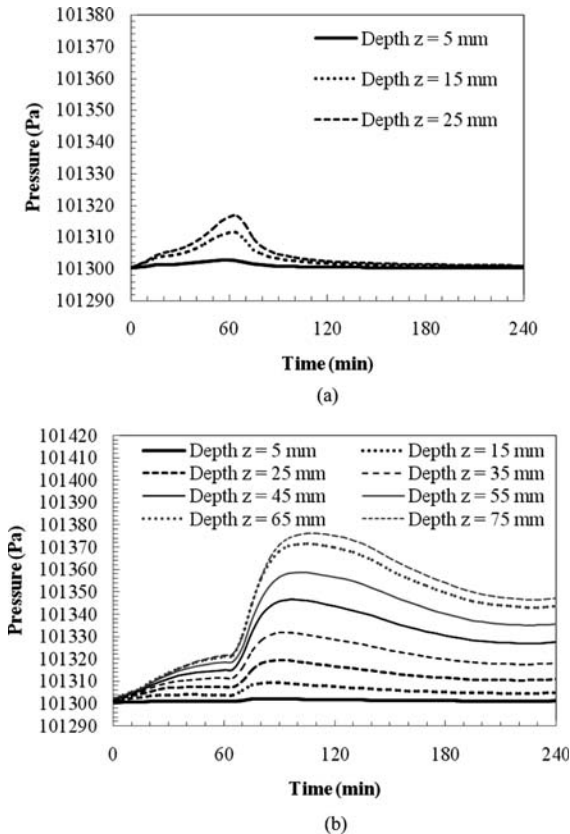


FIG. 12. Pressure profiles and time with different depths (F-bed): (a) sample thickness of 30 mm and (b) sample thickness of 80 mm.

Figures 10 and 11 show the numerical result of water saturation at various sample thicknesses (30, 50, and 80 mm). The results are linked between the temperature profiles and saturation profiles. High temperature gradient profiles lead to high rates of moisture evaporation and high water saturation profiles lead to higher temperature rise. On the other hand, a decrease of temperature gradient profiles leads to slow moisture evaporation and low water saturation profiles lead to lower thermal energy transformed.

As shown in Figs. 10a, 10b, and 11a, the effects of sample thickness strongly affect the temperature profiles and saturation profiles, particularly the thick packed bed because moisture content or water saturation is condensed near the bottom surface of the packed bed by gravitational force, whereas the upper surface always has lower saturation than the bottom surface. Therefore, moisture in the thick packed bed requires high thermal energy to evaporate and remain evaporated when it passes through the upper surface to the surrounding air. Furthermore, the thick packed bed has more water than the thin packed bed at the same water saturation and requires more thermal energy to evaporate the moisture content inside.

From Fig. 11, the effect of particle size on temperature profile is not clear, but it is prominent in water saturation profiles. This is because the small particle size has a higher capillary force than the large particle size, which strongly affects the fluid flow pattern and moisture distribution inside the sample.

Figures 12 and 13 show the numerical result of pressure profiles at various depths (30, 50, and 80 mm). The results are linked between the temperature profiles and pressure buildup profiles. The pressure buildup profile pattern is similar to the temperature profile pattern because there is a direct relationship between temperature and pressure gradients.

The effect of sample thickness directly affects the different pressure buildup profiles due to the temperature profile, which follows the distribution of electromagnetic field pattern, as seen in Figs. 12a, 12b, and 13a.

The effect of particle size is not only prominent in water saturation profiles but also clear in pressure buildup profiles, as seen in Fig. 13. This is because small particle size has greater capillary action than large particle size, which leads to a strong effect of flow pattern, resulting in stronger

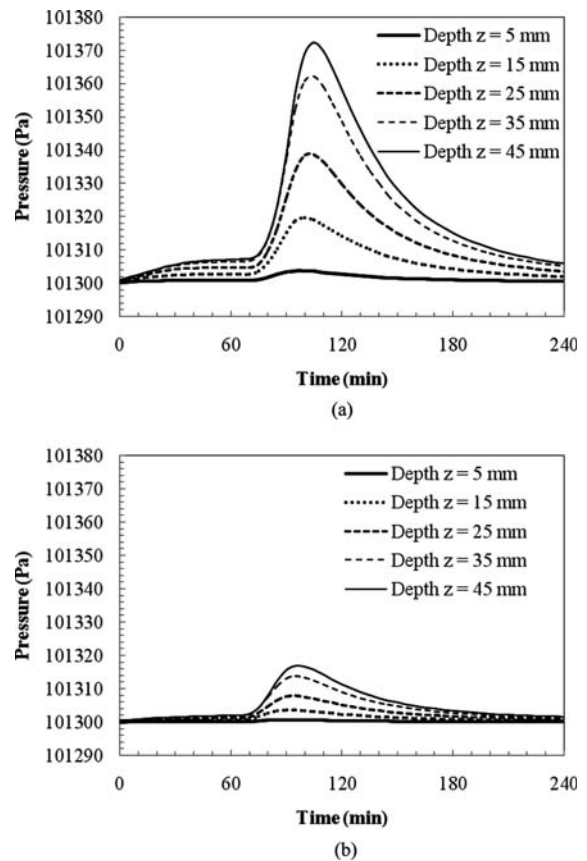


FIG. 13. Pressure profiles and time with different depths (sample thickness of 50 mm): (a) F-bed and (b) C-bed.

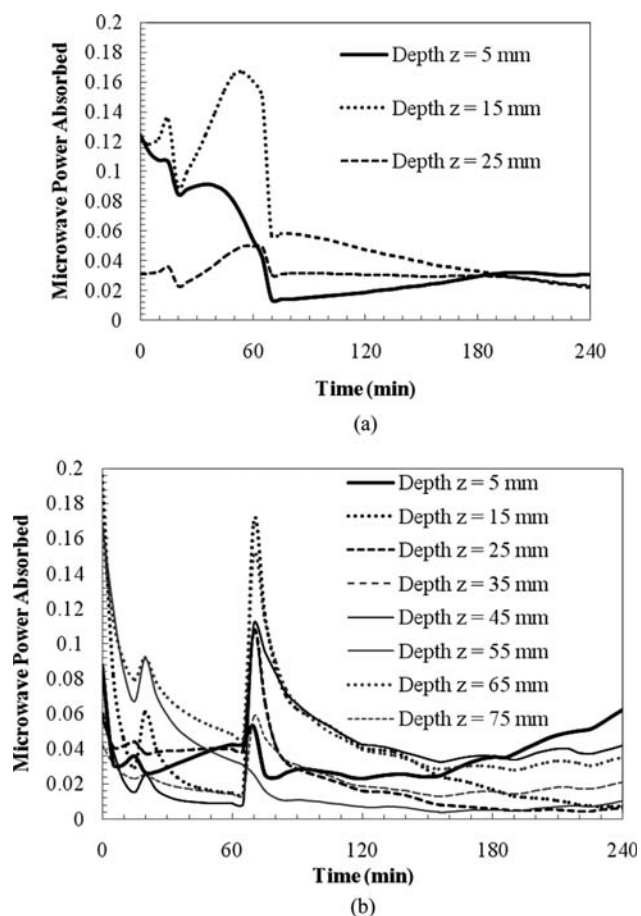


FIG. 14. Microwave power absorption profiles and time with different depths (F-bed): (a) sample thickness of 30 mm and (b) sample thickness of 80 mm.

pressure buildup profiles inside the small particle size packed bed.

Figures 14 and 15 show the numerical result of microwave power absorption profile versus elapsed times at various sample thickness (30, 50, and 80 mm). The results are linked between the temperature profiles and microwave power absorption profiles. This is because the microwave power absorbed is mainly electromagnetic heating, which is transformed from electromagnetic energy into thermal energy.

The effects of sample thickness are presented clearly in Figs. 14a, 15a, and 14b. The microwave power absorption profiles of thin layer packed beds differ from thick layer packed beds. This is because the sample size strongly affects the electromagnetic wave pattern inside the cavity. This explanation for this is similar to the temperature profile discussion previously.

From Fig. 15, the effects of particle size on microwave power absorption profiles is not clearly seen in a thick layer

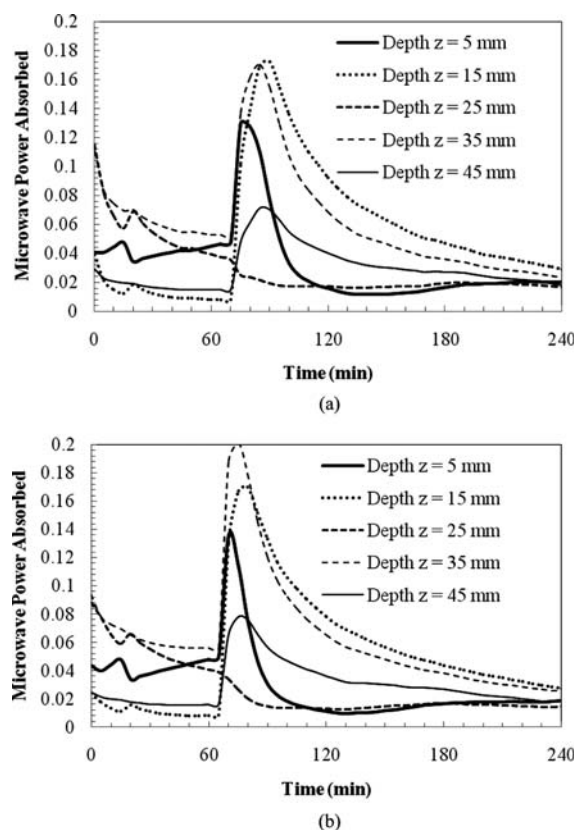


FIG. 15. Microwave power absorption profiles and time with different depths (sample thickness of 50 mm): (a) F-bed and (b) C-bed.

packed bed but is clearly seen in a thin layer packed bed due to the same reasons discussed for temperature profiles.

Figures 16 and 17 show the temperature distribution, water saturation distribution, and pressure buildup distribution in the case of an F-bed subject to microwave heating times of 10, 100, and 360 min, respectively. They display a wavy behavior and all cases of temperature distribution in packed beds of various thicknesses have cold and hot spot zones inside the samples. Furthermore, hot spot zones appear at the mid-plane near the bottom surface of the sample and cold spot zones appear at the wall of the waveguide near the upper surface of the sample. Additionally, the hot spot zone can be more than one point if the relationship between sample thickness and microwave penetration depth, directly corresponding to electromagnetic field patterns, is suitable for a strong standing wave effect.

The water saturation is strongly affected by temperature distribution as discussed in the previous section because the high temperature near the mid-plane of the sample leads to a higher driving force due to capillary flow and vapor diffusion, which cause moisture to migrate from hot spot zones to cold spot zones.

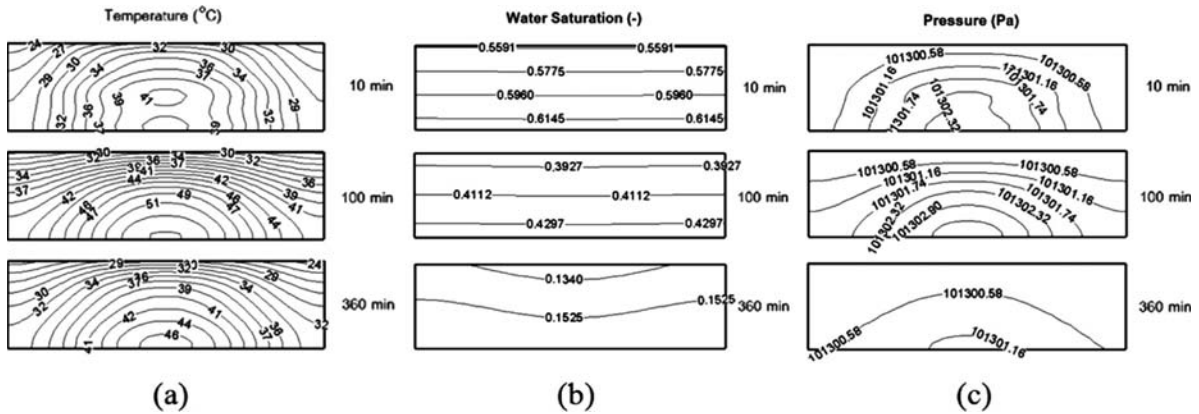


FIG. 16. Contour plot for F-bed (30 mm) at drying times of 10, 100, and 360 min: (a) temperature contour, (b) water saturation contour, and (c) pressure contour.

Temperature distribution not only affects water saturation but also pressure buildup distribution. A detailed explanation is given in the discussion on pressure buildup profiles.

Figures 18 and 19 show the fluid movements between the liquid and gas phases inside the packed bed in case of an F-bed at various heating times (10, 100, and 360 min). For the liquid flux vector, it can be observed that almost all of the liquid has migrated toward the upper surface of the sample due to capillary pressure and gas pressure buildup, which are simultaneously changed due to the effect of water saturation distribution and temperature distribution in each time period. For the case of 50-mm-thick samples, at heating time of 10 min there is less liquid movement due to the greater amount of saturated water inside the pores.

This is because most of the microwave energy is used to heat up the porous packed bed without a phase change at this stage. At a heating time of 100 min, liquid flux in large quantities moves to the upper surface due to the effect of pressure buildup, which is a function of temperature together with capillary action. However, the liquid flux rarely moves at the end of the heating time because the temperature inside the sample is decreased and liquid quantities are very low. For the case of an 80-mm-thick sample, the results for heating times of 10 and 100 min are similar to the previous cases, whereas at the end of heating they are different because water saturation and temperature are still high. On the other hand, the gas flux direction for all cases has different direction from liquid flux that corresponds to pressure buildup and temperature distribution.

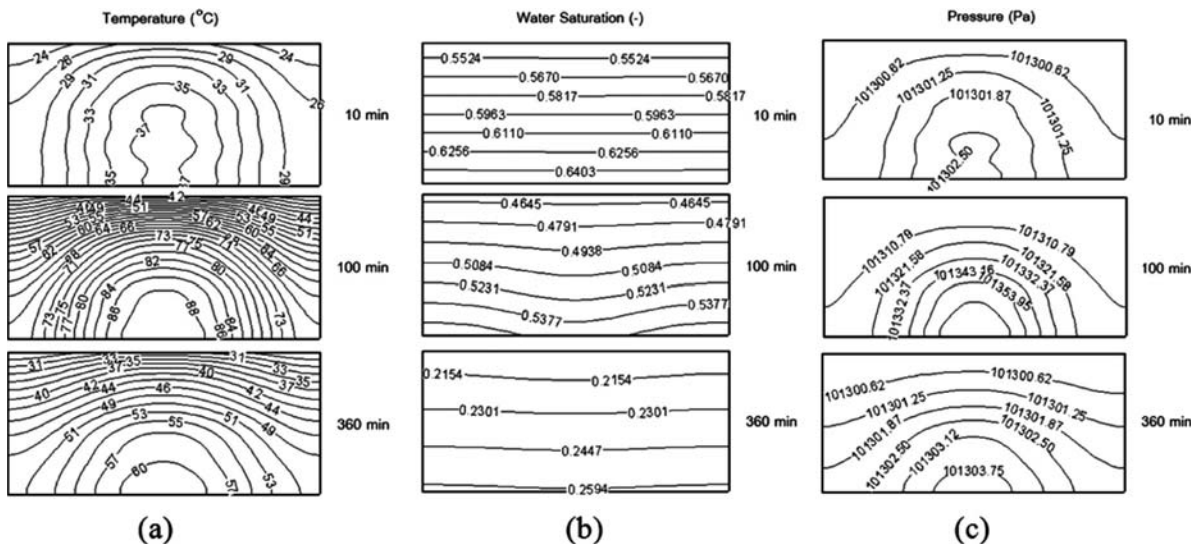


FIG. 17. Contour plot for F-bed (50 mm) at drying times of 10, 100, and 360 min: (a) temperature contour, (b) water saturation contour, and (c) pressure contour.

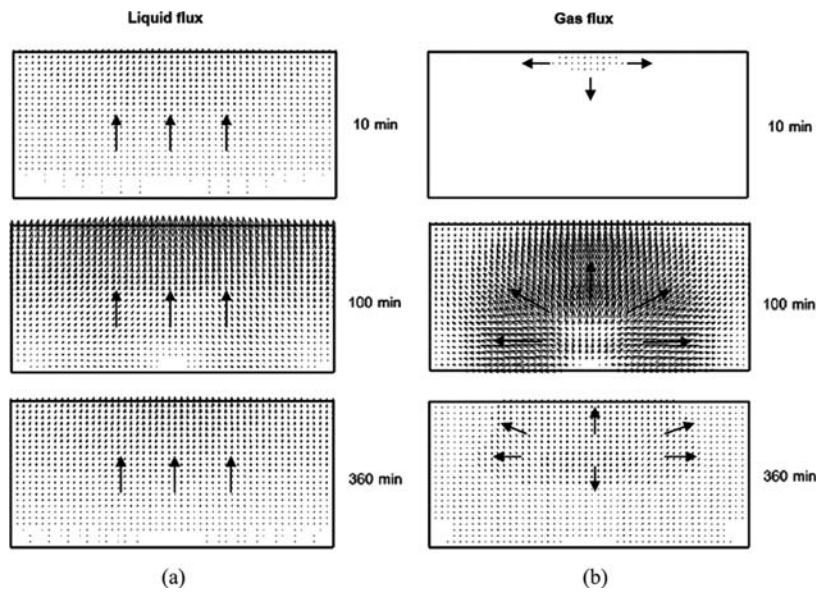


FIG. 18. Fluid movement pattern inside the F-bed (sample thickness of 50 mm) at heating times of 10, 100, and 360 min: (a) liquid flux (scale $\times 5,000$) and (b) gas flux (scale $\times 30,000,000$).

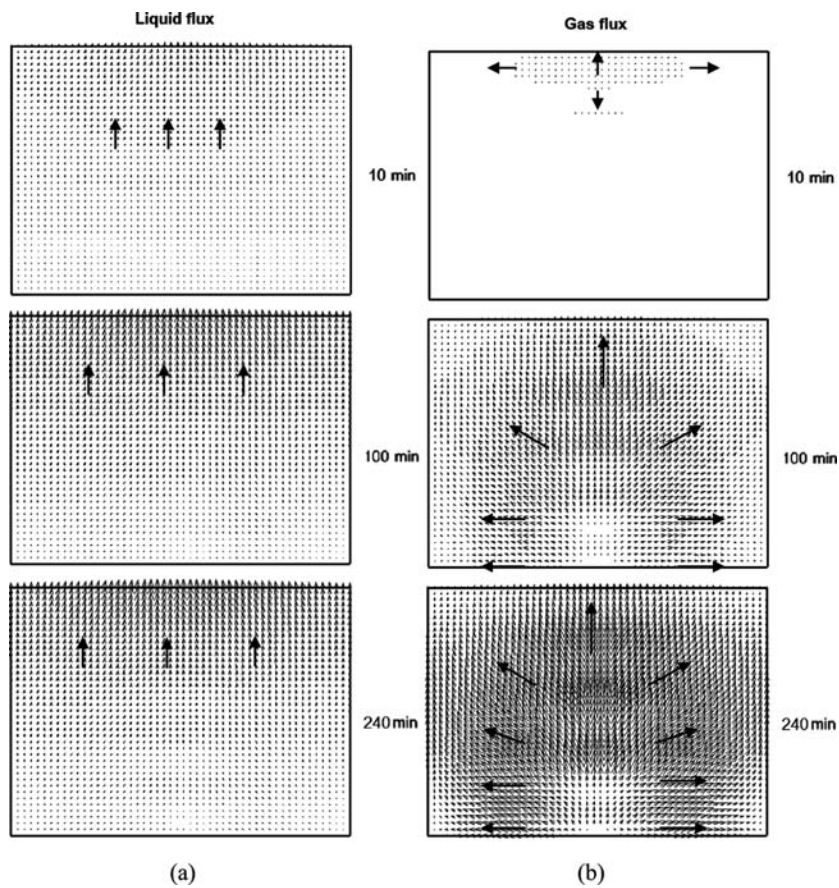


FIG. 19. Fluid movement pattern inside the F-bed (sample thickness of 80 mm) at heating times of 10, 100, and 360 min: (a) liquid flux (scale $\times 5,000$) and (b) gas flux (scale $\times 30,000,000$).

This is because the nonuniform temperature distribution leads to a discontinuous evaporation rate inside the sample, which induces a pressure explosion inside the sample. The gas flux, which is function of pressure buildup, is then moved because of these effects. Furthermore, the difference in temperature distribution of various sample thicknesses results in different patterns of liquid and gas flow.

CONCLUSION

The numerical analysis presented describes many important interactions within a single-layer porous packed bed with different particle sizes and different sample thicknesses during microwave heating using a rectangular waveguide. The following paragraphs summarize the conclusions of this study.

A mathematical model for analysis of heat and mass transfer and pressure buildup in typical porous packed beds subjecting to microwave energy can be used successfully to describe transport phenomena in several conditions.

The particle size significantly affects to describe pressure buildup distribution, water saturation distribution, and movement of fluid inside the unsaturated porous packed bed. In addition, the saturated distribution can change the electromagnetic field and heat and mass transfer patterns.

The sample thickness strongly influences heating behavior because it can change electromagnetic field patterns, microwave power absorption, and temperature distribution profile results.

The results in this work are useful in designing microwave drying and heating machines or to improve the product quality from microwave processes.

NOMENCLATURE

C_p	Specific heat capacity (J/kgK)
D_m	Effective molecular mass diffusion (m^2/s)
E	Electric field intensity (V/m)
f	Frequency (GHz)
g_r	Gravitational constant (m/s^2)
H	Magnetic field intensity (A/m)
H_v	Specific heat of vaporization (J/kg)
h_c	Heat transfer constant (W/m^2K)
h_m	Mass transfer constant (W/m^2K)
K	Permeability (m^2)
\dot{m}	Phase change term (kg/m^3s)
P	Microwave power (W)
p	Pressure (Pa)
Q	Microwave power absorbed term (W/m^3)
s	Water saturation
T	Temperature ($^{\circ}C$)
t	Time (s)
$\tan \delta$	Loss tangent coefficient
u, w	Velocity (m/s)

Greek Letters

ε	Complex permittivity (F/m)
ε'	Permittivity or dielectric constant
ε''	Dielectric loss factor
λ_{eff}	Effective thermal conductivity (W/mK)
μ	Magnetic permeability (H/m)
μ	Dynamic viscosity (Pa s)
ρ	Density (kg/m^3)
ϕ	Porosity

Subscripts

0	Free space
a	Air
c	Capillary
g	Gas
l	Liquid water
p	Particle
r	Relative
v	Water vapor
x, z	Coordinate axis (m)
∞	Ambient condition

ACKNOWLEDGMENT

The authors thank the Office of the Higher Education Commission, Thailand, for support of a grant fund under the program Strategic Scholarships for Frontier Research Network for the Joint Ph.D. Program Thai Doctoral degree and the National Research University Project of Thailand Office of Higher Education Commission.

REFERENCES

1. Ayappa, K.G.; Davis, H.T.; Davis, E.A.; Gordon, J. Analysis of microwave heating of materials with temperature-dependent properties. *AIChE Journal* **1991**, *37*, 313–322.
2. Saltiel, C.; Datta, A. Heat and mass transfer in microwave processing. *Advances in Heat Transfer* **1997**, *30*, 1–94.
3. Tada, S.; Echigo, R.; Kuno, Y.; Yochida, H. Numerical analysis of electro-magnetic wave in partially loaded microwave applicator. *International Journal of Heat and Mass Transfer* **1998**, *41*, 708–718.
4. Basak, T.; Meenakshi, A. A theoretical analysis on microwave heating of food slabs attached with ceramic plates: Role of distributed microwave incidence. *Food Research International* **2006**, *39*(8), 932–944.
5. Rattanadecho, P.; Suwannapum, N.; Chatveera, B.; Atong, D.; Makul, N. Development of compressive strength of cement paste under accelerated curing by using a continuous microwave thermal processor. *Materials Science and Engineering: A* **2008**, *472*(1–2), 299–307.
6. Kowalski, S.J.; Rajewska, K. Convective drying enhanced with microwave and infrared radiation. *Drying Technology* **2009**, *27*, 878–887.
7. Alibas, I. Microwave, vacuum, and air drying characteristics of collard leaves. *Drying Technology* **2009**, *27*, 1266–1273.
8. Perre, P.; Turner, I.W. Microwave drying of softwood in an oversized waveguide. *AIChE Journal* **1997**, *43*, 2579–2595.
9. Rattanadecho, P. The simulation of microwave heating of wood using a rectangular wave guide: Influence of frequency and sample size. *Chemical Engineering Science* **2006**, *61*(14), 4798–4811.
10. Bories, S.A. Fundamental of drying of capillary-porous bodies. In *Convective Heat and Mass Transfer in Porous Media*; NATO ASI

- Series; Kakac, S., Kilkis, B., Kulacki, F., Arinc, F., Eds.; Kluwer Publishers: New York, 1991; 196, 391–434.
11. Boukadida, N.; Ben Nasrallah, S. Two dimensional heat and mass transfer during convective drying of porous media. *Drying Technology* **1995**, *13*(3), 661–694.
 12. Curcio, S. A multiphase model to analyze transport phenomena in food drying processes. *Drying Technology* **2010**, *28*, 773–785.
 13. Rattanadecho, P.; Pakdee, W.; Stakulcharoen, J. Analysis of multiphase flow and heat transfer: Pressure buildup in an unsaturated porous slab exposed to hot gas. *Drying Technology* **2008**, *26*, 39–53.
 14. Ratanadecho, P.; Aoki, K.; Akahori, M. A numerical and experimental investigation of the modeling of microwave drying using a rectangular wave guide. *Drying Technology* **2001**, *19*(9), 2209–2234.
 15. Campañone, L.A.; Zaritzky, N.E. Mathematical analysis of microwave heating process. *Journal of Food Engineering* **2005**, *69*(3), 359–368.
 16. Knoerzer, K.; Regier, M.; Schubert, H. A computational model for calculating temperature distributions in microwave food applications. *Innovative Food Science & Emerging Technologies* **2008**, *9*(3), 374–384.
 17. Cha-um, W.; Rattanadecho, P.; Pakdee, W. Experimental analysis of microwave heating of dielectric materials using a rectangular wave guide (MODE: TE₁₀) (case study: Water layer and saturated porous medium). *Experimental Thermal and Fluid Science* **2009**, *33*(3), 472–481.
 18. Rattanadecho, P.; Suwannapum, N.; Cha-um, W. Interactions between electromagnetic and thermal fields in microwave heating of hardened type I-cement paste using a rectangular waveguide (influence of frequency and sample size). *ASME Journal of Heat Transfer* **2009**, *131*, 082101–082112.
 19. Hansson, L.; Antti, L. Modeling microwave heating and moisture redistribution in wood. *Drying Technology* **2010**, *26*, 552–559.
 20. Jia, D.; Afzal, M.T. Modeling the heat and mass transfer in microwave drying of white oak. *Drying Technology* **2008**, *26*, 1103–1111.
 21. Ratanadecho, P.; Aoki, K.; Akahori, M. Influence of irradiation time, particle sizes and initial moisture content during microwave drying of multilayered capillary porous materials. *ASME Journal of Heat Transfer* **2002**, *124*(1), 151–161.
 22. Wang, J.; Schmugge, T. An empirical model for the complex dielectric permittivity of soil as a function of water content. *IEEE Transactions on Geosciences and Remote Sensing* **1980**, *18*, 288–295.
 23. Whitaker, S. A theory of drying in porous media. *Advances in Heat Transfer* **1977**, *13*, 119–203.
 24. Patankar, S.V. *Numerical Heat Transfer and Fluid Flow*; Hemisphere Publishing Corporation: New York, 1980.